Physics of the Earth and Planetary Interiors 256 (2016) 37–48

Contents lists available at ScienceDirect

Physics of the Earth and Planetary Interiors

journal homepage: www.elsevier.com/locate/pepi

Anisotropic Rayleigh wave tomography of Northeast China using ambient seismic noise

Zhikun Liu [a,b,*], Jinli Huang [a,b], Huajian Yao [c,d]

[a] School of Geophysics and Information Technology, China University of Geosciences, Beijing 100083, China
[b] Key Laboratory of Geo-detection (China University of Geosciences, Beijing), Ministry of Education, 100083, China
[c] Laboratory of Seismology and Physics of Earth's Interior, School of Earth and Space Sciences, University of Science and Technology of China, Hefei 230026, China
[d] National Geophysical Observatory at Mengcheng, Anhui, China

ARTICLE INFO

Article history:
Received 4 February 2016
Received in revised form 27 April 2016
Accepted 1 May 2016
Available online 6 May 2016

Keywords:
Surface waves
Azimuthal anisotropy
Ambient noise tomography
Northeast China
Songliao basin

ABSTRACT

The ambient noise data recorded by 249 seismic stations in the permanent and temporary networks in Northeast China are used to invert for the isotropic phase velocity and azimuthal anisotropy of Rayleigh waves in the period band 5–50 s. The inversion results reflect the structure from the shallow crust to upper mantle up to approximately 120 km depth. Beneath the Songliao basin, both the fast direction in shallow crust and strike of a low-velocity anomaly in the middle crust are NNE–SSW, which is coincident with the main tectonic trend of the (Paleo) Pacific tectonic domain. This indicates that the rifting of the Songliao basin is influenced by the subduction of (Paleo) Pacific plate. The upper mantle of Songliao block (except the central area of Songliao basin) to the west of Mudanjiang fault, and the east of the North–South Gravity Lineament, is characterized by high-velocity and weak anisotropy up to approximately 120 km depth. We infer that there is delamination of lithospheric mantle beneath the Songliao block. Obvious N–S, NE–SW, and E–W trending fast directions are found in the lithospheric mantles of the east, west, and south sides of Songliao block, respectively, which coincide with the strikes of the Paleozoic tectonic in these areas. This suggests that the frozen-in anisotropic fabric in the lithospheric mantle can be used to indicate the historical deformation of the lithosphere. In the northern margin of the North China Craton, the spatial variations of phase velocity and azimuthal anisotropy are more dramatic than those in Northeast China blocks, which indicates that the lithosphere of the North China Craton has experienced more complicated tectonic evolution than that of the Northeast China blocks.

1. Introduction

Northeast China includes part of the eastern section of the Central Asian Orogenic Belt (CAOB) and the northern margin of the North China Craton (NCC) (Li, 2006). With the Chifeng–Kaiyuan fault (CKF) as a boundary, the northern part belongs to the eastern section of the CAOB, including micro blocks such as the Xing'an, Songliao, and Jiamusi blocks (Fig. 1). There have been controversies regarding the evolution of these blocks and the collision of them with the Siberia Craton to the north and the NCC to the south (Zhou and Wilde, 2013); however, in general, this region was controlled by the Paleo-Asian Ocean tectonic domain in the Paleozoic and the (Paleo) Pacific Ocean tectonic domain since the Mesozoic (Wu et al., 2011). Meanwhile, this region was likely to be influenced by the subduction of the Mongolia-Okhotsk Ocean plate during the Mesozoic (Xu et al., 2013). The large-scale sedimentary basins such as Songliao basin (SB) (Wei et al., 2010) and the extensive intra-plate volcanic activities (Wang et al., 2006) generated since the Mesozoic–Cenozoic are related to the complicated tectonic settings. To investigate the tectonic evolution, and the relationship between the shallow geological features and deep structures in Northeast China, it is important to use the seismological method to constrain the structure and deformation characteristics of the lithosphere.

In some studies of large-scale body wave tomography, the structures of upper mantle in Northeast China were investigated and stagnant slabs were imaged in the mantle transition zone (*e.g.*, Huang and Zhao, 2006; Li and van der Hilst, 2010); however, the structures of lithosphere in this areas are not constrained well from body wave tomography because and teleseismic body wave tomography could not provide better vertical resolution within the lithosphere (*e.g.*, Lei and Zhao, 2005). Surface wave

* Corresponding author at: School of Geophysics and Information Technology, China University of Geosciences, Beijing 100083, China. Tel.: +86 10 82321446.
E-mail address: zkliu@cugb.edu.cn (Z. Liu).

http://dx.doi.org/10.1016/j.pepi.2016.05.001
0031-9201/

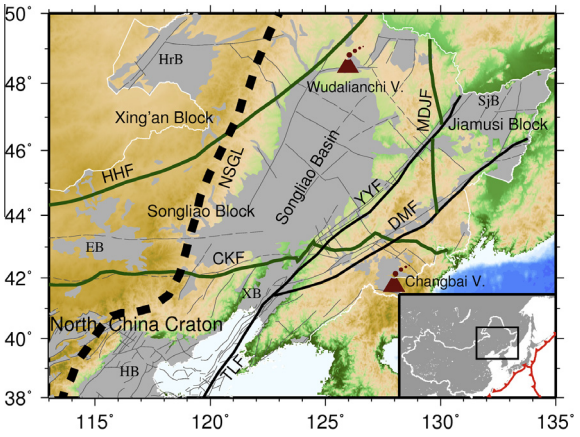

Fig. 1. Topography and tectonic settings of Northeast China. The dark green lines indicate the boundary lines of the main tectonic units in Northeast China. CKF, the Chifeng–Kaiyuan fault; MDJF, the Mudanjiang fault; HHF, the Hegenshan–Heihe fault. The thick dashed line in black represents the North–South Gravity Lineament (NSGL). The thick black lines denote the Tancheng–Lujiang fault (TLF) and its two branches in Northeast China. YYF, the Yilan–Yitong fault; DMF, the Dunhua-Mishan fault. The thin black lines represent active faults. The gray areas represent sedimentary basins. HrB, the Hailar basin; SjB, the Sanjiang basin; EB, the Erlian basin; XB, the Xialiaohe basin; HB, the Huabei basin. The red triangles denote volcanoes. Wudalianchi V, the Wudalianchi volcano; Changbai V, the Changbaishan volcano. The inset figure shows the locations of the study region (black box). The abbreviation in the text: NCC, the North China Craton; SB, the Songliao basin; SLB, the Songliao block; JB, Jiamusi block. (For interpretation of the references to colour in this figure legend, the reader is referred to the web version of this article.)

tomography is another tool used in determining the structure of the lithosphere in Northeast China and its surrounding regions (*e.g.*, Huang et al., 2003; Priestley et al., 2006; Li et al., 2012). In addition, the seismic anisotropy derived from surface wave could offer constraints on the past and present deformation in the lithosphere and asthenosphere (*e.g.*, Montagner and Tanimoto, 1991; Huang et al., 2004, 2015; Yao et al., 2010; Isse et al., 2010; Legendre et al., 2014). In Northeast China, Li and Niu (2010) probed the seismic anisotropy in the mantle by SKS wave splitting. However, SKS splitting measurement is weakly sensitive to the distribution of anisotropy with depth. Analysis of surface waves can provide the distributions of azimuthal seismic anisotropy both laterally and vertically, thus it is important to study the anisotropic structure of Northeast China using surface waves. Traditional earthquake-based surface wave analysis, however, typically does not yield reliable measurements at short periods (<20 s). Recent developments in ambient noise tomography avoid the limitation of the distribution of earthquakes and can be favourably utilized to constrain crust and upper mantle structures (*e.g.*, Shapiro et al., 2005; Yao et al., 2006, 2010; Yang et al., 2007; Lin et al., 2011; Zheng et al., 2011).

The coverage of seismic stations is relatively sparse in Northeast China until the deployment of the NECESSArray (Northeast China Extended SeiSmic Array) during 2009–2011, which has greatly enhanced capabilities of seismological research in this region. Tang et al. (2014) conducted teleseismic P- and S-wave tomography, and investigated the formation mechanism of the Changbaishan volcano by using data recorded by the NECESSArray and seismic arrays in surrounding areas. Tao et al. (2014) revealed the crustal thickness and Poisson's ratio in the study area by using the receiver function. Liu et al. (2015) investigated the structure of the transition zone of the mantle beneath Northeast China. Guo et al. (2015) obtained the velocity structure of the S-wave in the crust by joint inversion of the receiver function and the dispersion data from ambient seismic noise. In this study, we invert both the isotropy and azimuthal anisotropy of Rayleigh wave phase velocity structures in Northeast China using continuous seismic data from NECESSArray and the permanent stations of Chinese regional networks, and discuss their tectonic implications.

2. Data and method

2.1. Data

During the period of September 2009 to August 2011, 127 broadband seismic stations were deployed in the area spanning 116°–134° E and 43°–48° N in Northeast China with an average separation of 80 km. This was subject to an international cooperation project NECESSArray supported by China, the United States, and Japan (Tang et al., 2014).

We collect the continuous waveforms of the vertical components of 124 seismic stations with good continuity from the NECESSArray and those of 125 seismic stations from Chinese regional networks (Zheng et al., 2010) in the same time period (Fig. 2). Compared with previous work using ambient seismic noise tomography (*e.g.*, Guo et al., 2015), we use more data from the intensively distributed China regional networks in the south of the NECESSArray. The study area is extended southwards, so that the structure and deformation of the lithosphere in the NCC and Northeast China blocks can be compared.

2.2. Ambient noise cross-correlation and dispersion measurements

The pre-processing of ambient seismic noise for a single station is mainly carried out according to the procedure proposed by Bensen et al. (2007). Firstly, the continuous seismic waveforms are decimated to five samples *per* second, followed by the instrument response correction. Then, the mean value and linear trend are removed before the waveforms are band-pass filtered in the period band 2–100 s. Then, we perform temporal normalization using a running-absolute-mean method and spectrum whitening. The waveforms of the ambient seismic noise from each station can be obtained thereby. Then, the Welch's method is used to calculate the cross-correlation of the ambient seismic noise (Seats et al., 2012). Finally, all the cross-correlation waveforms for each station pair during the study period are stacked and the empirical Green's functions are obtained by taking the time derivative of the cross-correlation waveforms (Sabra et al., 2005; Yao et al., 2006).

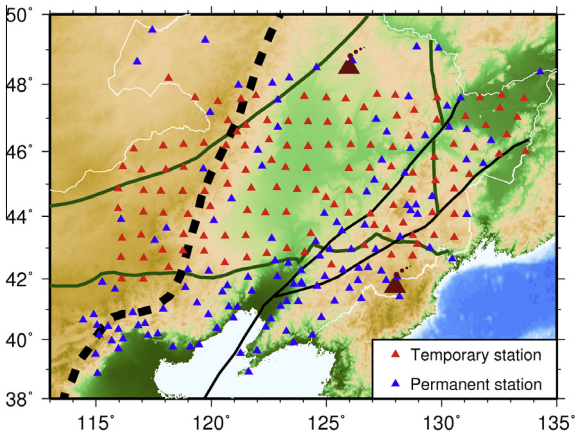

Fig. 2. Distribution of the seismic stations used in this study. The blue and red triangles represent permanent stations of Chinese regional networks and the temporary stations of the NECESSArray, respectively. The other legend entries match those in Fig. 1. (For interpretation of the references to color in this figure legend, the reader is referred to the web version of this article.)

The method, based on image analysis (Yao et al., 2006), is used to extract the dispersion curves of Rayleigh wave phase velocity. To ensure the reliability of the measurement for the dispersion curves, only those measurements with a signal to noise ratio (SNR) greater than five for each period are retained. The SNR is defined as the ratio of the maximum amplitude within the signal window (determined by the station spacing and the group velocity range of 2–5 km/s) to the average amplitude within the noise window (150 s-length waveform right after the signal window). We also perform spatial cluster analyses on the measurements of phase velocity dispersion (Bensen et al., 2007) to remove outliers in the measurements. Since 249 seismic stations are used in this study, there should ideally be 30,876 measurements for each period. After the aforementioned quality control procedures are applied, the numbers of the phase velocity measurements retained at each period are shown in Fig. 3. As shown, the numbers of phase velocity measurements with periods shorter than 35 s are all above 10,000, while those with periods longer than 35 s decrease rapidly due to the use the far-field approximation of surface wave representation for dispersion analysis (Yao et al., 2006). Although there are only 1653 measurements at the period of 50 s, the path coverage is good for most of the study area.

2.3. Inversion of the isotropic Rayleigh wave phase velocity and azimuthal anisotropy

In a weak anisotropic medium, the local azimuthally varying phase velocity of the surface wave can be expressed by a Fourier series (Smith and Dahlen, 1973):

$$c(T,M,\psi) = c_0(T)(1 + a_0(T,M) + a_1(T,M)\cos 2\psi + a_2(T,M)\sin 2\psi + a_3(T,M)\cos 4\psi + a_4(T,M)\sin 4\psi) \quad (1)$$

where T is the period of velocity and $c_0(T)$ indicates the reference phase velocity, which is usually the average value of all observed phase velocities at this period, ψ is the angle between the wave vector and due north, a_0 and $a_i (i = 1–4)$ represent the perturbation of the isotropic phase velocity and azimuthally anisotropic coefficients, respectively. In a weak anisotropic medium, 4ψ terms contribute little to the phase velocity of the Rayleigh wave and therefore can be ignored. Hence, we only invert for the perturbation of the isotropic phase term a_0 and the azimuthally anisotropic terms a_1 and a_2 in this study. The magnitude of azimuthal anisotropy A_c and the fast direction Θ can be obtained using the following formulae

$$A_c(T,M) = \sqrt{a_1^2(T,M) + a_2^2(T,M)} \quad (2)$$

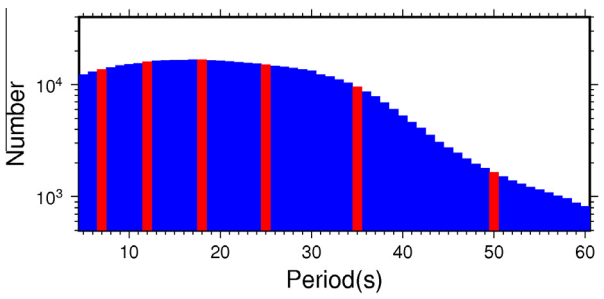

Fig. 3. Numbers of the phase velocity measurements at different periods. The red vertical bars indicate the periods given in the tomography maps in Fig. 6. (For interpretation of the references to colour in this figure legend, the reader is referred to the web version of this article.)

$$\Theta = \frac{1}{2}\arctan\left(\frac{a_2}{a_1}\right) \quad (3)$$

We use the continuous regionalization (Montagner, 1986) based on the generalized inversion scheme (Tarantola and Valette, 1982) to invert for both isotropic and azimuthally anisotropic phase velocity maps. The inversion is mainly controlled by three parameters including the standard error of phase velocity measurements σ_d, the *a priori* parameter error σ_p and the spatial correlation length L. σ_p and L are constraints for the anomaly amplitude and the smoothness of model parameters, respectively.

The standard error σ_d is 1% for all measured values of the phase velocity according to previous analyses on bias of phase velocity measurements from ambient noise cross-correlations (*e.g.*, Yao and van der Hilst, 2009). After conducting an extensive series of tests and residual analyses, we determine the key inversion parameters as follows. With respect to the isotropic coefficient a_0, *a priori* error σ_p is set to be twice of the standard deviation of the observed phase velocity at each period. As for the anisotropic coefficients a_1 and a_2, σ_p is set to be 1% of the average value of the phase velocity at each period. The choices of the spatial correlation length L are period dependent. For isotropic terms, L varies from 50 km to 150 km with the period in the range of 5 s to 50 s, while for the anisotropic term, L is set to twice that of the isotropic term at the corresponding period.

2.4. Resolution test

A checkerboard test is usually used to assess the spatial resolution in tomographic models. For the isotropic part, we construct a synthetic phase velocity model with ±6% velocity perturbations of the average velocity for each period. Then, the synthetic travel times are calculated with an additional 1% random error. Finally, we invert the synthetic data by using the same method and parameters as with the real data to obtain the recovery model. Taking the period of 25 s as an example, Fig. 4 demonstrates the $1^\circ \times 1^\circ$ phase velocity checkerboard model and the recovered model. As seen, the perturbation pattern and amplitude of the model are recovered in most of the study area. However, the model in the northwest margin is not well retrieved because of the poor path coverage.

In the checkerboard test of azimuthal anisotropy, we construct an input model with an anisotropic strength of 2% and fast directions of ±45°alternately. The calculation of synthetic travel times and the inversion are same as those in the isotropic case. Owing to the correlation length of the anisotropic term being twice that of the isotropic term in the inversion process, the anomaly scale of the input model is set to twice that of the isotropic checkerboard at the corresponding period. Taking a period of 25 s for instance, the $2^\circ \times 2^\circ$ checkerboard input model and the recovery results are shown in Fig. 5. The magnitude of azimuthal anisotropy and the fast direction are usually well recovered in regions with dense station distribution. However, the anisotropy at the margins is poorly recovered, which is caused by sparse path coverage as well as the smoothing effect at the grid boundaries.

We test the checkerboard with different sized grids for each period in this study. We find that for periods shorter than 35 s, the $2^\circ \times 2^\circ$ checkerboard model of azimuthal anisotropy can be favourably recovered. As for longer periods (such as 50 s), although the number of measurements decrease, the $3^\circ \times 3^\circ$ checkerboard achieve good recovery in most of the study area.

3. Results

Based on the aforementioned methods, the isotropic phase velocity and azimuthal anisotropy of Rayleigh waves with periods varying from 5 s to 50 s are obtained in the study area. Figs. 6–8

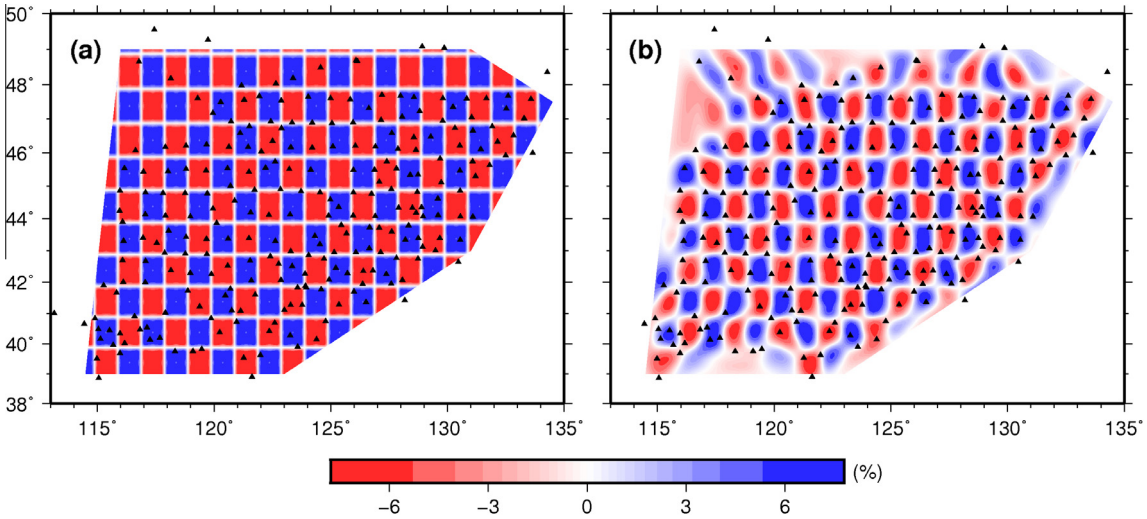

Fig. 4. Checkerboard resolution test (anomaly size 1° × 1°) of the isotropic phase velocity at a period of 25 s. (a) and (b) represent the input model and recovery results, respectively. The black triangles indicate the seismic stations.

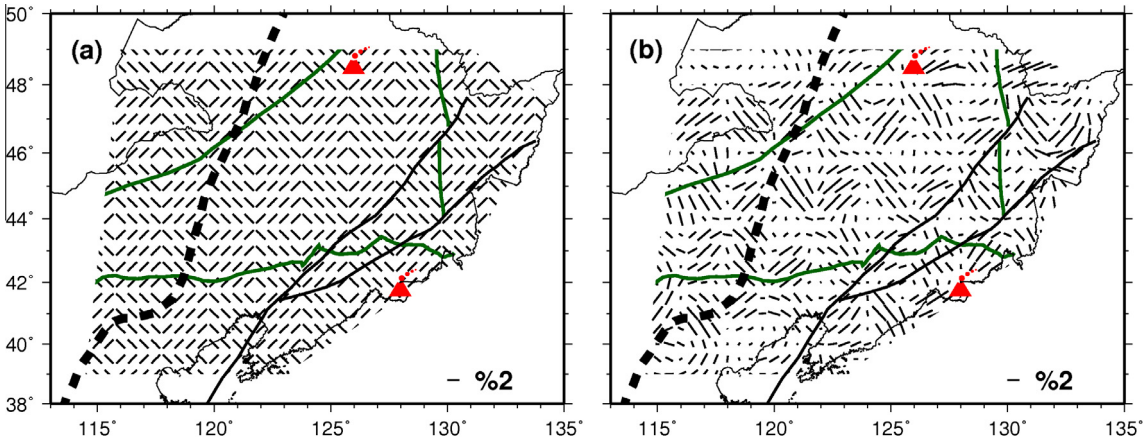

Fig. 5. Checkerboard resolution test (anomaly size 2° × 2°) of azimuthal anisotropy at a period of 25 s. (a) and (b) represent the input model and the recovery results, respectively, and the rest of legends are the same as those in Fig. 1.

show the anisotropic phase velocity maps and corresponding posterior errors at six periods in Northeast China.

The posterior error is a useful guide to assess the extent to which the inversion is resolved from the data. In regions where the posterior error is much smaller than the *a prior* error, the resolution is better, while in the regions where the posterior error nearly equals the *a prior* error, the resolution is poor (Tarantola and Valette, 1982). As shown in Figs. 7 and 8, in the most of study areas the posterior errors of isotropic phase velocity and magnitude of azimuthal anisotropy are less than 2% and 0.6%, respectively. The posterior errors are lower compared to the *a prior* errors therein (about 10% to 15% and 4% to 5.5%, respectively), which indicates that good resolution is achieved in this study. Thus the boundaries of tomographic maps are restricted by some contours of posterior error (*e.g.*, 2% to 3%) of the isotropic phase velocity in Fig. 6. In addition, the posterior errors are smaller than the perturbation of isotropic phase velocities and the magnitude of the azimuthal anisotropy (Fig. 6). This also demonstrates the reliability of our inversion results.

The Rayleigh wave phase velocities of different periods are mainly sensitive to shear velocity structures at different depths (*e.g.*, Liu et al., 2014) and the sensitivity kernels are shown in Fig. 9. In the study areas, the phase velocities at periods of 7 s and 12 s are most sensitive to shear velocity structures of the upper crust at depths of 5–10 km and 9–16 km, respectively. With increasing period, the range of sensitive depths of the phase velocity becomes broader. The phase velocities at periods of 18 s and 25 s may reflect structures of the middle-lower crust and around the crust-mantle boundary. The phase velocities at longer periods are sensitive to the upper mantle structure and a period of 50 s could reflect the information of the lithospheric mantle up to 120 km depth.

3.1. Isotropic phase velocity of Rayleigh waves

The image of the phase velocity at a period of 7 s mainly reveals the shear velocity structure of the shallow crust at depths from 5 to 10 km. This phase velocity map is closely related to the regional geological structures including the thickness of the sedimentary layers and the depth of the crystalline basement. Fig. 10 shows that the boundaries of the low-velocity anomalies at a period of 7 s could clearly depict the major sedimentary basins in Northeast China including the Songliao, Xialiaohe, Sanjiang, and Hailar basins (Fig. 10b). Obvious high-velocity anomalies are found in mountainous areas, such as Daxing'anling.

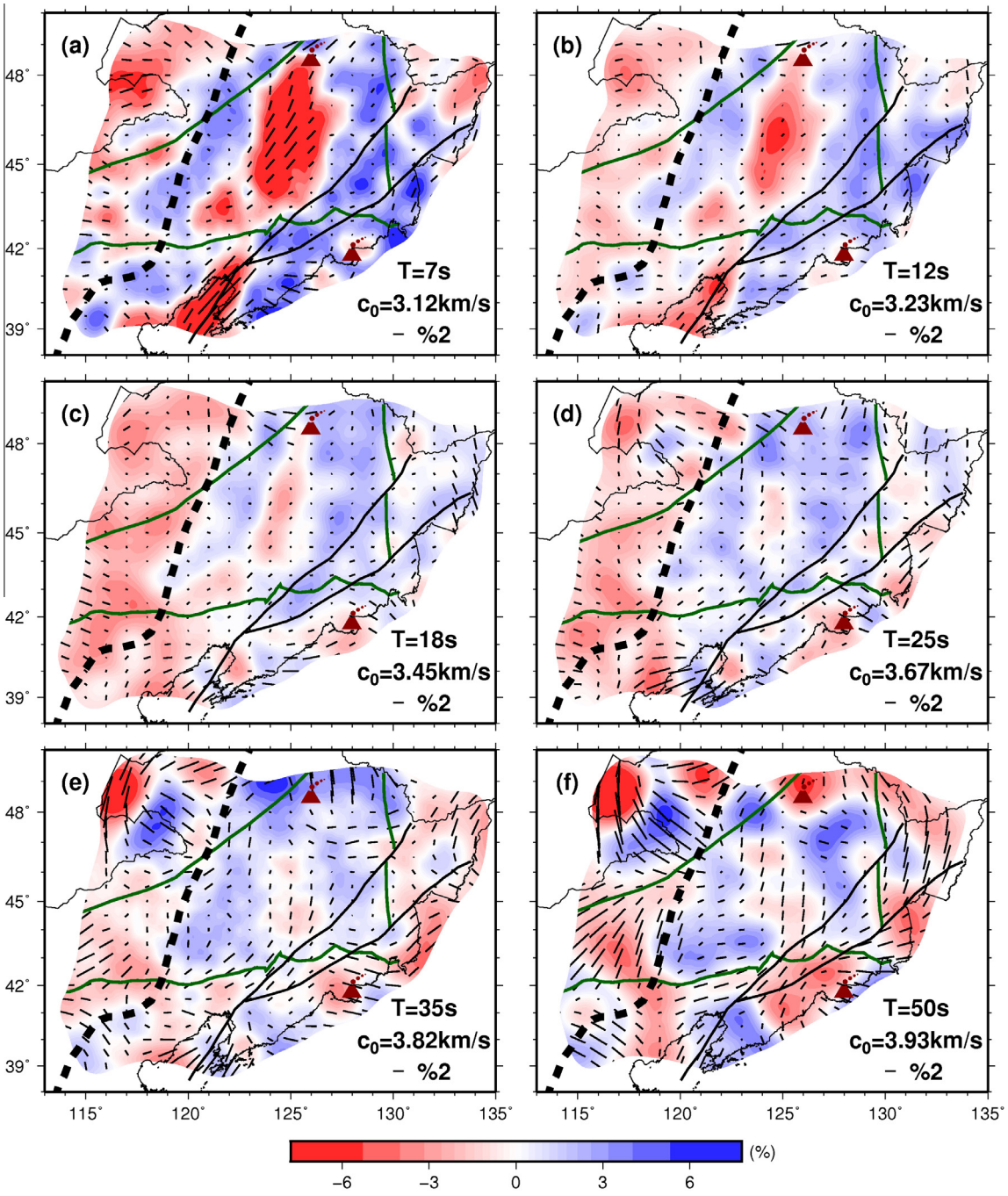

Fig. 6. Variation of isotropic phase velocities and azimuthal anisotropy of Rayleigh waves at different periods. The period and the corresponding reference velocity, *i.e.* the average value of the phase velocity at that period, are labeled in the lower right corner of each panel. The velocity perturbation scale in per cent with respect to the reference velocity is shown at the bottom. The length of the black bar represents the magnitude of the azimuthal anisotropy and its scale is labeled in the lower right corner of each panel. The direction of the bar represents the fast direction. The other legend entries match those in Fig. 1.

The phase velocities at periods of 12 s (Fig. 6b) and 18 s (Fig. 6c) reflect the variations of the velocity structures in the middle-lower crust at depths of about 9–16 km and 12–24 km, respectively. With increasing period, the impact of the surface structure on the distribution of the phase velocity is gradually weakened. Bounded by the North–South Gravity Lineament (NSGL), the broad western areas are characterized by low velocities, while the Songliao block (SLB) to the east exhibits a high-velocity anomaly on the whole, except in the central area of SB, which is endowed with a low-velocity anomaly probably due to the effect of thick sediments nearly 10 km.

At a period of 25 s, the phase velocity reflects the structure at a depth of between 25 and 40 km, which is about the range of Moho depths in Northeast China. In Fig. 11 we compare the distribution of the phase velocity at 25 s and the crustal thickness from the CRUST1.0 model (Laske et al., 2013). The phase velocities at the east and west sides of the NSGL are dominated by the positive and negative velocity anomalies, respectively (Fig. 11a), which

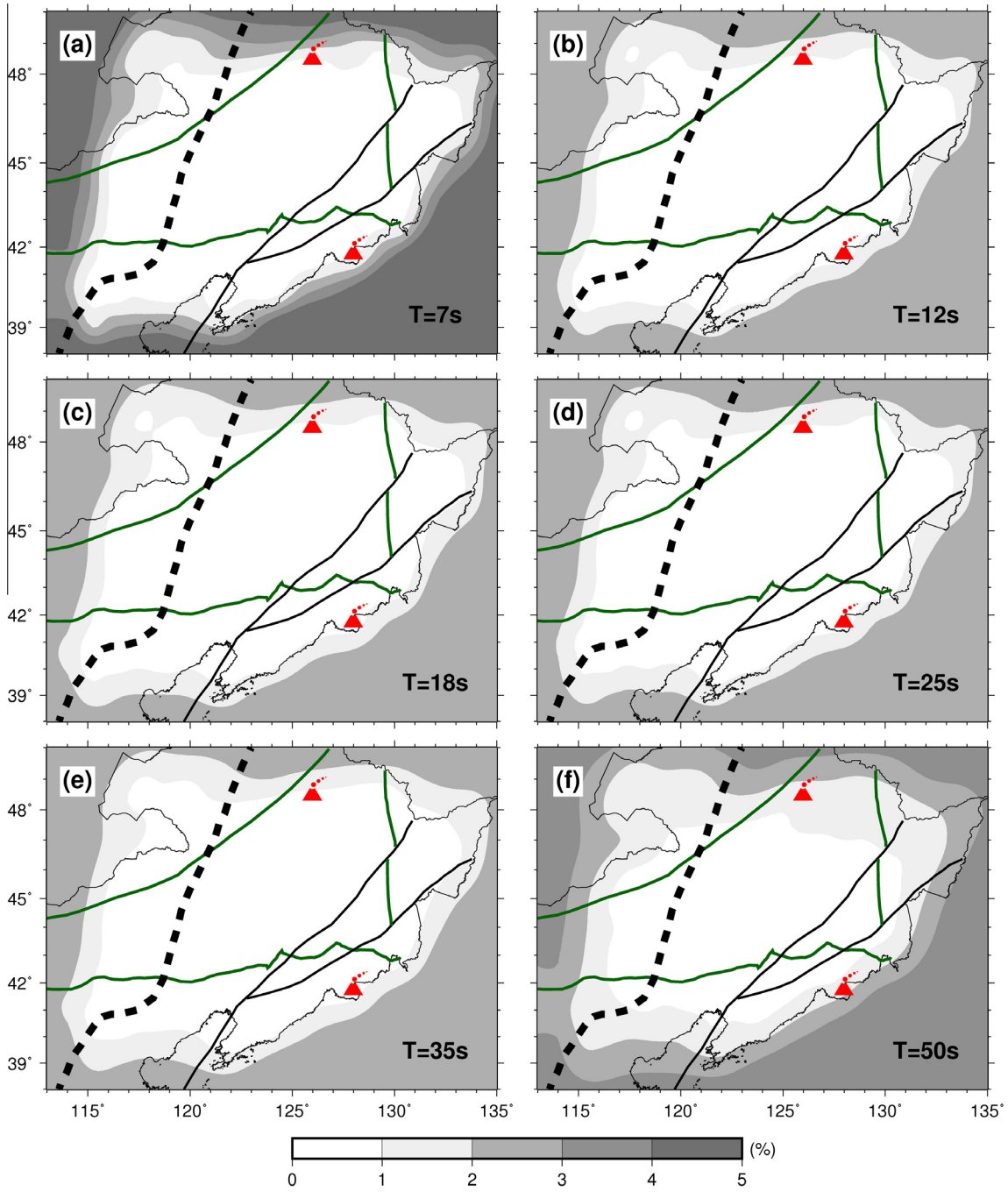

Fig. 7. Posterior errors of the isotropic phase velocity of Rayleigh waves at different periods.

can favourably reflect the relative thick and thin Moho depths on the two sides, respectively (Fig. 11b). The phase velocities underneath the SB, Changbaishan, and the middle and north segments of the Dunhua-Mishan fault present relatively low velocities, corresponding to deeper Moho beneath these areas.

As to the phase velocities at periods of 35 s (Fig. 6e) and 50 s (Fig. 6f), they are sensitive to the velocity structures of the lithospheric mantle approximately 40–80 km depth and up to 120 km depth, respectively. The results reveal that there is also a velocity difference across the two sides of the NSGL, and that the phase velocity within the NCC is generally lower than that in the Northeast China blocks.

3.2. Azimuthal anisotropy of the Rayleigh wave

To analyze the variations of azimuthal anisotropy with depth (period), we select five representative profiles along the longitude or latitude in the study area (Fig. 12a) and plot the measurements of the azimuthal anisotropy with more periods beneath the profiles (Fig. 12b–f) than in Fig. 6.

At a period of 7 s, the most obvious characteristic is the strong NNE–SSW fast direction appearing in the Songliao and Xialiaohe basins (Fig. 6a). According to the data along profiles A–A′ (Fig. 12b) and C–C′ (Fig. 12d), the strong azimuthal anisotropy is limited to within periods of less than 10 s. The results at a period of 12 s

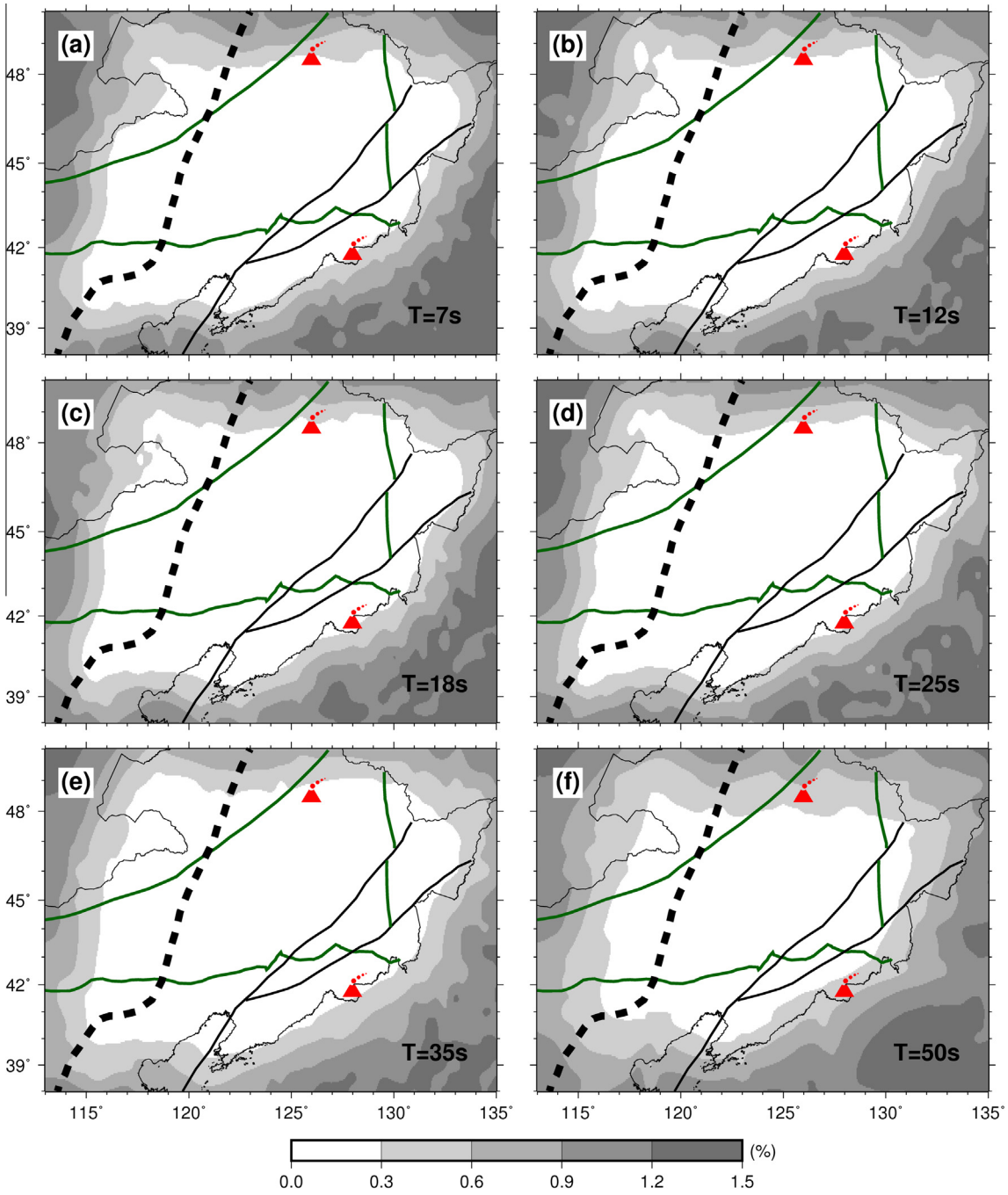

Fig. 8. Posterior errors of the magnitude of the azimuthal anisotropy of Rayleigh waves at different periods.

(Fig. 6b) and 18 s (Fig. 6c) show that the azimuthal anisotropy in the middle-lower crust of the study area as a whole is weak. At a period of 25 s (Fig. 6d), the magnitude of the anisotropy is generally greater, which indicates that the anisotropy around the crust-mantle boundary is stronger than that in the middle-lower crust. At this period, there is observable anisotropy in the boundary of the Northeast China blocks and the NCC, and the fast direction is almost parallel to the strike of the CKF.

The anisotropy at periods of 35 s (Fig. 6e) and 50 s (Fig. 6f) could reflect the deformation characteristics of the lithospheric mantle. As seen in Fig. 12, both the magnitude and fast direction vary greatly at the two sides of the boundary lines of tectonic units, such as the NSGL, MDJF, and CKF. In general, although the anisotropy of the SLB to the east of the NSGL is relatively weak, obvious N–S, NE–SW, and E–W trending fast directions are found in the east, west, and south sides of the SLB, respectively.

4. Discussion

The isotropic phase velocity and the azimuthal anisotropy of the Rayleigh wave were obtained in this study, reflecting structural heterogeneity and deformation styles from the shallow crust to the upper mantle up to 120 km depth in Northeast China. The phase velocity is mainly sensitive to the shear wave velocity of the medium, and may be related to the thermal state, material composition, and filled fluid properties thereof. The driving factors behind the azimuthal anisotropy are complicated. It is generally

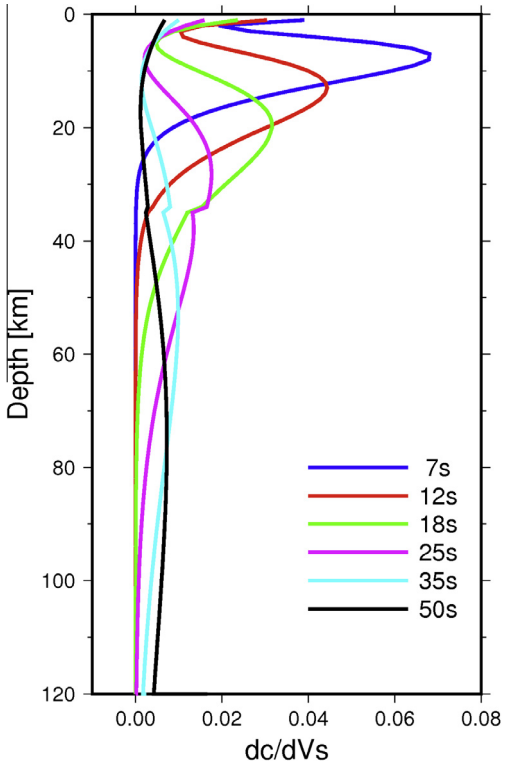

Fig. 9. Rayleigh wave phase velocity sensitivity kernels at different periods.

belived that the anisotropy of the shallow crust is mainly determined by the orientations of the fractures, and the fast direction is similar to the strike of the fault (Balfour et al., 2005). The anisotropy of the lower crust and the upper mantle result from the lattice preferred orientation (LPO) of amphibole and olivine, respectively. When a certain finite strain accumulates under the same deformation pattern, the direction of the fast wave tends to be coincident with the direction of the maximum extension for pure shear deformation or shear direction for simple shear deformation (Savage, 1999). Lithospheric mantle is mainly composed of olivine, and its anisotropy can be preserved for a long time during tectonic periods. Thus, the seismic anisotropy of the lithosphere can be used to deduce its historical tectonic deformation and interaction process with neighboring blocks, whereas the anisotropy of the asthenosphere may just reflect the contemporary mantle flow (Long and Becker, 2010). Since the phase velocity obtained in this study almost cannot detect the information at the depth of asthenosphere, we mainly focus on the study of the structure and deformation of lithosphere in Northeast China.

4.1. Songliao basin (SB) and Songliao block (SLB)

SB is the largest oil production area and rift basin in China, as well as the center of the late Mesozoic rifting and lithospheric thinning in eastern China (Ren et al., 2002). It is widely believed that SB has experienced four evolution stages including: asthenosphere upwelling, extensional rifting, cooling depression, and tectonic inversion (Feng et al., 2010). The evolution stages reflect the complicated tectonic background including two tectonic domains: the Paleo-Asian Ocean and the (Paleo) Pacific Ocean. There have been disputes regarding the geodynamic mechanism of the SB, especially concerning the subduction system that controls the rifting process. Some studies argued that it was mainly caused by the (Paleo) Pacific plate (*e.g.*, Ren et al., 2002; Zhang et al., 2011) while some believed that the subduction of the Mongolia-Okhotsk plate was the main driving force (*e.g.*, Meng, 2003; Wei et al., 2010).

In our study, the boundary of the low-velocity anomaly at a period of 7 s clearly describes the outline of the basin (Fig. 10). Moreover, the variation of the magnitude of the velocity can indicate variations in the thickness of the sedimentary layer. For example, the lowest phase velocity at a period of 12 s is found in the central area of the SB, which corresponds to the central depression with the thickest sedimentary layer nearly 10 km (Feng et al., 2010). The low-velocity anomaly beneath SB is divided into two parts, the southwestern and northern SB, respectively (Fig. 6a and b). In addition, both magnitude of azimuthal anisotropy and fast direction differ between the southwestern and northern part of SB. These observations indicate that the two areas have experienced different tectonic evolution and sedimentary histories (Wei et al., 2010).

The shallow crust of SB exhibits a prominent NNE–SSW fast direction at the depth less than 10 km (Figs. 6a and 12). At the same depth range, 3-D seismic surveys revealed a series of NNE–SSW normal faults and fault blocks due to the extensional

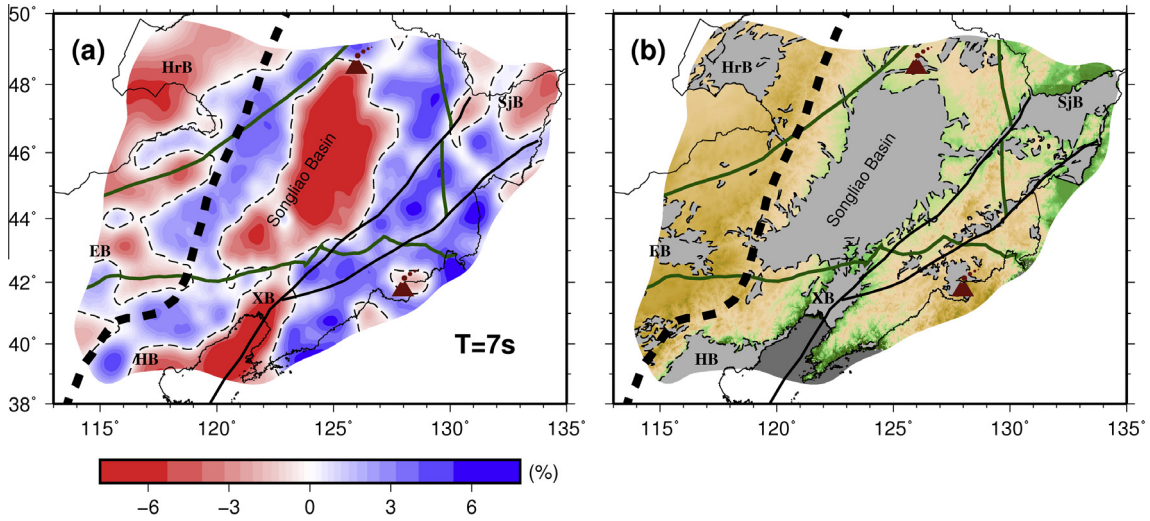

Fig. 10. Rayleigh wave phase velocities at a period of 7 s (a) and the distribution of sedimentary basins (gray color) in the study area (b). The abbreviations used to denote the basins match those used in Fig. 1.

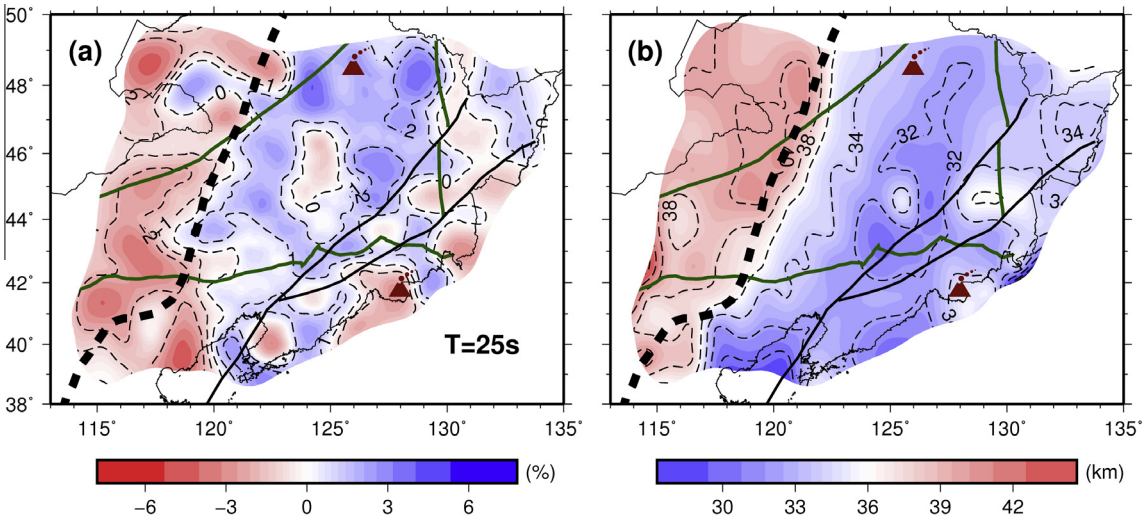

Fig. 11. Rayleigh wave phase velocity at a period of 25 s (a) and the crustal thickness in the study area (b).

tectonism during the rifting period of SB (Feng et al., 2010; Wei et al., 2010). Thus, we argue that the anisotropy in the shallow crust results from the fractures due to extensional rifting of SB. We also find a remarkable low-velocity anomaly having a similar strike with the NNE–SSW trending rift basin in the middle crust beneath the SB (Fig. 6c), which may be related to the upwelling process of hot materials from the mantle in an active rift model or the decompression melting process in a passive rift model (Cloetingh and Ziegler, 2007). Both the fast direction in the shallow crust, and the strike of the low-velocity anomaly in the middle crust, are NNE–SSW, which is similar with the tectonic trend in the study region in its (Paleo) Pacific tectonic domain (Ren et al., 2002). It is possible that the rifting of SB was significantly influenced by the (Paleo) Pacific tectonic processes.

Although the central area of SB presents a low-velocity anomaly from the middle-lower crust to the upper mantle, the Songliao block (SLB) to the west of the MDJF and the east of the NSGL exhibits a high-velocity anomaly on the whole. The uplifting of the Moho in this area (Tao et al., 2014; Zhang et al., 2014) could be an explanation for the high-velocity at a period of 25 s (Fig. 11). For longer periods, we also observe remarkable high-velocity anomaly beneath the SLB. Guo et al. (2016) find the high-velocity anomaly may extend to at least 200 km depth. Previous studies (*e.g.*, Li et al., 2012) reveal that the thickness of the lithosphere beneath SLB is approximately 70–80 km. Thus, the high-velocity anomaly deeper than this depth (*e.g.*, at a period of 50 s, Fig. 6f) may be a reflection of the submergence of the high-velocity lithospheric mantle into the low-velocity asthenospheric mantle. If this were true, the lithospheric delamination is supposed to occur after the Mesozoic. This is because the lithospheric mantle of the SLB, to the east of NSGL, is represented by weak azimuthal anisotropy, which is different from the obvious frozen-in anisotropy (next section) preserved in the neighboring blocks. This suggests that information relating to historical deformation in the lithosphere of SLB before the Mesozoic was possibly erased by later lithospheric process.

4.2. The west of the North–South Gravity Lineament (NSGL)

The North–South Gravity Lineament (NSGL) is an important geological zone in eastern China. The morphology, gravity and magnetic anomalies, crustal and lithospheric thickness (Zheng et al., 2006; Chen and Ai, 2009), as well as the mantle geochemistry (Xu, 2007) all change considerably across the NSGL.

Our results indicate that the west of the NSGL is basically characterized by a low-velocity anomaly at the depth of the middle-lower crust (Fig. 6c and d), which is roughly consistent with the area where the Mesozoic and Cenozoic volcanic rocks are widely distributed (Xu et al., 2013). Deep seismic sounding also demonstrates the existence of the curved reflection phases of the igneous rock in the lower crust under this region (Hou et al., 2015). Therefore, the low-velocity anomaly in the middle-lower crust is supposed to be a reflection of the magmatic activities (Kang et al., 2016).

The SLB to the east of the NSGL exhibits weak anisotropy in the lithospheric mantle, while that to the west of the NSGL presents strong NE-SW azimuthal anisotropy (Fig. 6c and d, and Fig. 12b and c). The NE-SW fast direction is similar to the strike of collision zone between the Siberia Craton and the NCC in this area in the Paleozoic, thus the observed anisotropy may be an indicator of frozen-in structure within the lithosphere. Moreover, it is also observed that both isotropic phase velocity and azimuthal anisotropy differ across the two sides of the Hegenshan–Heihe fault (HHF), the suture zone between the Xing'an and Songliao blocks (Wu et al., 2011). This may be a fundamental cause of the different lithospheric evolutions in the northern and southern areas of Daxing'anling (Zhang et al., 2010).

4.3. Jiamusi block (JB)

The Jiamusi block (JB) is one of the important tectonic units in Northeast China, but its tectonic attributes remain controversial. Oh (2006) believed that JB derived from the Yangtze plate, while Wu et al. (2011) thought that JB was possibly an exotic terrane from Gondwana. Based on data from the metamorphic core complex in Heilongjiang, Zhou and Wilde (2013) deduced that JB rifted away some 260 Ma and then re-docked with the SLB again at approximately 180–210 Ma.

Our results show that from the middle-lower crust to the upper mantle (12–35 s) the isotropic phase velocity is different on the two sides of the MDJF, which is the boundary of the JB and SLB. This may reflect different material properties and thermal states of the two blocks. In addition, the fast direction and magnitude of anisotropy in lithospheric mantle vary greatly at the two sides. The whole JB exhibits strong N–S trending azimuthal anisotropy (Fig. 12b), which is similar to that found in a previous large-scale anisotropic surface wave tomography study (Huang et al., 2004). Since the anisotropy does not merely occur near the suture zones

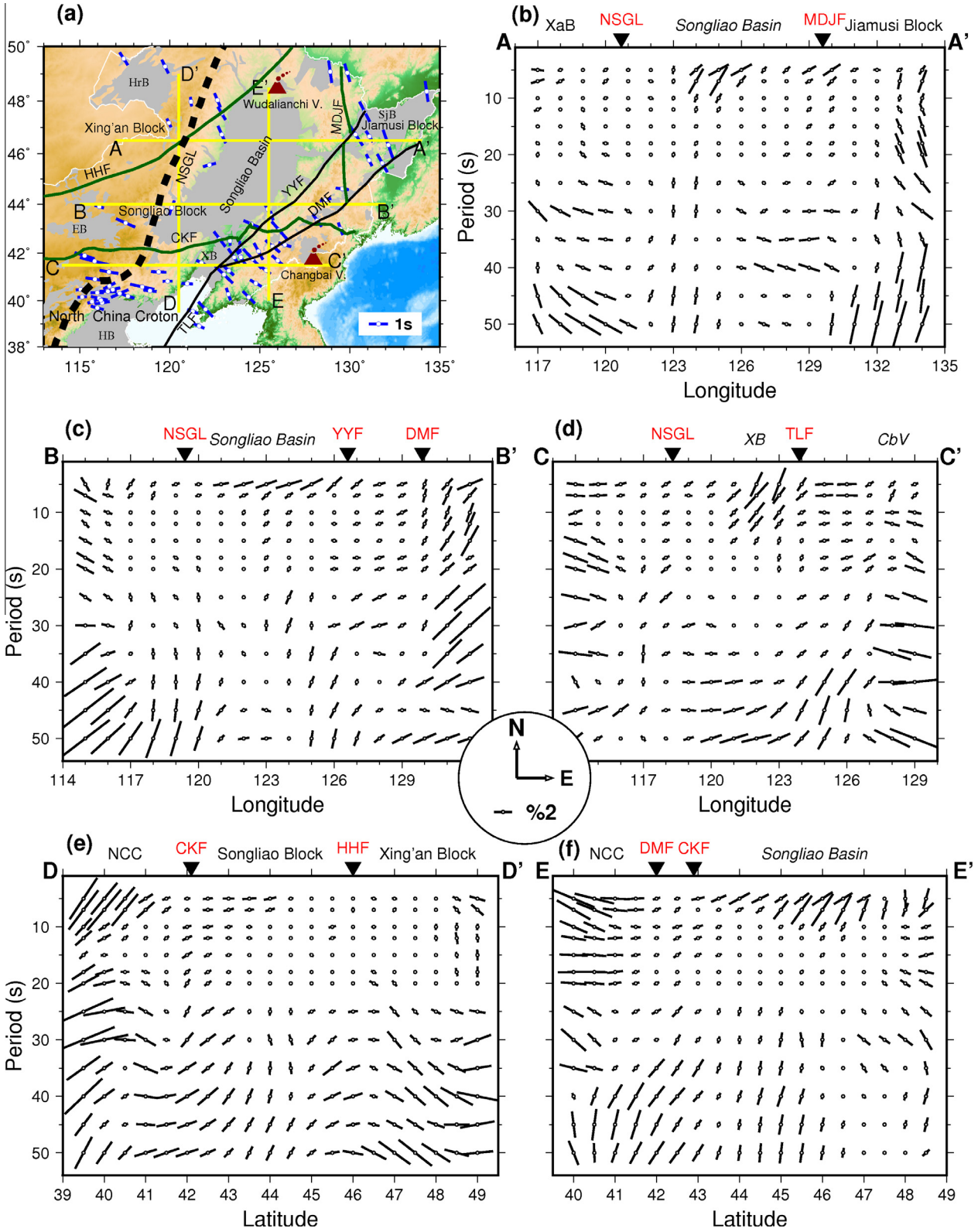

Fig. 12. Variations of the azimuthal anisotropy with period (b–f) under the five profiles whose locations are shown in (a). The shear wave splitting measurements (Li and Niu, 2010) are also shown in (a). The direction and length of blue bars represent the fast direction and splitting time, respectively. In (b–f), the upward and rightward directions of the bar represent the northward and eastward fast direction of Rayleigh wave. The length of the bar represents the magnitude of the azimuthal anisotropy, the scale of which is demonstrated within the circle. Abbreviation: XaB, the Xing'an block; CbV, the Changbaishan volcano. (For interpretation of the references to colour in this figure legend, the reader is referred to the web version of this article.)

between blocks, it is demonstrated that the strong anisotropy is not caused by collision between the blocks, but is influenced by the specific N–S trending tectonic setting. Thus, it is speculated that JB is possibly an exotic terrane due to the different physical

attributes and tectonic settings between the JB and the blocks to its west.

4.4. The northern margin of the North China Craton (NCC)

It is generally believed that Northeast China blocks were jointed with NCC in the late Permian-early Triassic, while the suture zone is located to the north of the CKF (Wu et al., 2011). In the suture zone, there is an observable azimuthal anisotropy around the crust mantle boundary (at a period of 25 s) with a NEE–SWW fast direction, which is similar to the strike of the CKF This local anisotropy may reflect the deformation in the lower crust and the top of the upper mantle caused by continental collision (*e.g.*, Deschamps et al., 2008).

Compared with the Northeast China blocks to the north of the CKF, the isotropic phase velocity beneath NCC exhibits more dramatic spatial variations (Fig. 6d–f)), which indicates the more heterogeneous lithospheric structure in the NCC. Moreover, the variations in azimuthal anisotropy of NCC with periods are more complex than those in the Northeast China blocks (Fig. 12e and f). This demonstrates that the lithosphere of the NCC has experienced more complicated tectonic evolution than that in the Northeast China blocks.

The nearly E–W fast direction in the lithospheric mantle is observed in the northern margin of the NCC (Fig. 6f), in which the strike is consistent with the Paleozoic tectonic trend in this region (Li, 2006). However, the magnitude of anisotropy or fast direction changes near the NSGL and the Changbaishan region, which may indicate that the originally tectonic structures were reformed by the formation of the NSGL in the Mesozoic (or even later) and the Changbaishan in the Cenozoic. The study of SKS wave splitting (Fig. 12a) also evinced the near-E–W fast directions in the northern margin of the NCC (Li and Niu, 2010), which may indicate that the lithospheric mantle contributes to the observed splitting to a greater extent than other layers such as the asthenosphere in this region.

5. Conclusion

In this study, we use ambient noise data recorded at 249 stations in Northeast China to construct the isotropic phase velocity maps and azimuthal anisotropy of Rayleigh waves with periods varying from 5 to 50 s. The inversion results reflect the structure from the shallow crust to upper mantle up to ~120 km depth. The fast direction in the shallow crust (with a period of less than 10 s) of Songliao basin is NNE–SSW trended. Meanwhile, an obvious low-velocity anomaly with similar strike is found in the middle crust, which may reflect the extensional rifting of Songliao basin as influenced by the tectonic settings of the (Paleo) Pacific Ocean. Except for the central area of Songliao basin, the whole Songliao block to the west of Mudanjiang fault and the east of North–South Gravity Lineament in low crust and lithospheric mantle is characterized by high velocity and weak anisotropy. It is speculated that there was lithospheric delamination beneath Songliao block since the Mesozoic. The widely distributed low-velocity anomalies found in the middle-lower crust to the west of the North–South Gravity Lineament are mainly caused by intense magmatic activities in the Mesozoic and Cenozoic. The prominent N–S fast direction in the lithospheric mantle of Jiamusi block is very different from that of other blocks in Northeast China, which indicates that the Jiamusi block is possibly an exotic terrane. Both isotropic phase velocity and azimuthal anisotropy beneath North China Craton exhibit more dramatic spatial variations than those in Northeast China blocks. This demonstrates that the lithosphere of the North China Craton has experienced a more complicated tectonic evolution than that in the Northeast China blocks.

Acknowledgements

We thank Necessarray Project Team for providing the waveform data of temporary seismic stations. Data of the permanent stations are provided by Data Management Center of China National Seismic Network at Institute of Geophysics, China Earthquake Administration (SEISDMC, doi:10.11998/SeisDmc/SN), and Earthquake Administration of Inner Mongolia, Jilin and Liaoning Province. We thank Jikun Feng at USTC for his help in the inversion program. We also thank the Editor (Vernon Cormier) and an anonymous reviewer for their comments. This study is supported by the National Natural Science Foundation of China (NO. 91114205 and 41304063), the Open Fund (NO. GDL1401) of Key Laboratory of Geo-detection (China University of Geosciences, Beijing), Ministry of Education, and the Fundamental Research Funds for the Central Universities (WK2080000053).

References

Balfour, N.J., Savage, M.K., Townend, J., 2005. Stress and crustal anisotropy in Marlborough, New Zealand: evidence for low fault strength and structure-controlled anisotropy. Geophys. J. Int. 163, 1073–1086. http://dx.doi.org/10.1111/j.1365-246X.2005.02783.x.

Bensen, G.D., Ritzwoller, M.H., Barmin, M.P., Levshin, A.L., Lin, F., Moschetti, M.P., Shapiro, N.M., Yang, Y., 2007. Processing seismic ambient noise data to obtain reliable broad-band surface wave dispersion measurements. Geophys. J. Int. 169, 1239–1260. http://dx.doi.org/10.1111/j.1365-246X.2007.03374.x.

Chen, L., Ai, Y., 2009. Discontinuity structure of the mantle transition zone beneath the North China Craton from receiver function migration. J. Geophys. Res. 114, B06307. http://dx.doi.org/10.1029/2008JB006221.

Cloetingh, S., Ziegler, P.A., 2007. Tectonic models of sedimentary basins. In: Schubert, G. (Ed.), Treatise on Geophysics. Elsevier, pp. 485–611, doi:10.1016/B978-044452748-6.00109-7.

Deschamps, F., Lebedev, S., Meier, T., Trampert, J., 2008. Azimuthal anisotropy of Rayleigh-wave phase velocities in the east-central United States. Geophys. J. Int. 173, 827–843. http://dx.doi.org/10.1111/j.1365-246X.2008.03751.x.

Feng, Z., Jia, C., Xie, X., Zhang, S., Feng, Z., Cross, T.A., 2010. Tectonostratigraphic units and stratigraphic sequences of the nonmarine Songliao basin, northeast China. Basin Res. 22, 79–95. http://dx.doi.org/10.1111/j.1365-2117.2009.00445.x.

Guo, Z., Chen, Y.J., Ning, J., Feng, Y., Grand, S.P., Niu, F., Kawakatsu, H., Tanaka, S., Obayashi, M., Ni, J., 2015. High resolution 3-D crustal structure beneath NE China from joint inversion of ambient noise and receiver functions using NECESSArray data. Earth Planet. Sci. Lett. 416, 1–11. http://dx.doi.org/10.1016/j.epsl.2015.01.044.

Guo, Z., Chen, Y.J., Ning, J., Yang, Y., Afonso, J.C., Tang, Y., 2016. Seismic evidence of on-going sublithosphere upper mantle convection for intra-plate volcanism in Northeast China. Earth Planet. Sci. Lett. 433, 31–43. http://dx.doi.org/10.1016/j.epsl.2015.09.035.

Hou, H., Wang, H., Gao, R., Li, Q., Li, H., Xiong, X., Li, W., Tong, Y., 2015. Fine crustal structure and deformation beneath the Great Xing'an Ranges, CAOB: revealed by deep seismic reflection profile. J. Asian Earth Sci. http://dx.doi.org/10.1016/j.jseaes.2015.01.030.

Huang, J., Zhao, D., 2006. High-resolution mantle tomography of China and surrounding regions. J. Geophys. Res. Solid Earth 111, 1–21. http://dx.doi.org/10.1029/2005JB004066.

Huang, T.-Y., Gung, Y., Kuo, B.-Y., Chiao, L.-Y., Chen, Y.-N., 2015. Layered deformation in the Taiwan orogen. Science 349, 720–7233. http://dx.doi.org/10.1126/science.aab1879.

Huang, Z., Su, W., Peng, Y., Zheng, Y., Li, H., 2003. Rayleigh wave tomography of China and adjacent regions. J. Geophys. Res. 108, 2073. http://dx.doi.org/10.1029/2001JB001696.

Huang, Z., Peng, Y., Luo, Y., Zheng, Y., Wei, S., 2004. Azimuthal anisotropy of Rayleigh waves in East Asia. Geophys. Res. Lett. 31, 1–4. http://dx.doi.org/10.1029/2004GL020399.

Isse, T., Shiobara, H., Montagner, J.-P., Sugioka, H., Ito, A., Shito, A., Kanazawa, T., Yoshizawa, K., 2010. Anisotropic structures of the upper mantle beneath the northern Philippine Sea region from Rayleigh and Love wave tomography. Phys. Earth Planet. Inter. 183, 33–43.

Kang, D., Shen, W., Ning, J., Ritzwoller, M.H., 2016. Seismic evidence for lithospheric modification associated with intracontinental volcanism in Northeastern China. Geophys. J. Int. 204, 215–235. http://dx.doi.org/10.1093/gji/ggv441.

Laske, G., Masters, G., Ma, Z., Pasyanos, M., 2013. Update on CRUST1.0 – A 1-degree Global Model of Earth's Crust. EGU Gen. Assem. Conf. Abstr. 15, 2658.

Legendre, C.P., Deschamps, F., Zhao, L., Lebedev, S., Chen, Q., 2014. Anisotropic Rayleigh wave phase velocity maps of eastern China. J. Geophys. Res. Solid Earth 119, 4802–4820. http://dx.doi.org/10.1002/2013JB010781.Received.

Lei, J., Zhao, D., 2005. P-wave tomography and origin of the Changbai intraplate volcano in Northeast Asia. Tectonophysics 397, 281–295. http://dx.doi.org/10.1016/j.tecto.2004.12.009.

Li, C., van der Hilst, R.D., 2010. Structure of the upper mantle and transition zone beneath Southeast Asia from traveltime tomography. J. Geophys. Res. 115, B07308. http://dx.doi.org/10.1029/2009JB006882.

Li, J., Niu, F., 2010. Seismic anisotropy and mantle flow beneath northeast China inferred from regional seismic networks. J. Geophys. Res. Solid Earth 115, 1–17. http://dx.doi.org/10.1029/2010JB007470.

Li, J.-Y., 2006. Permian geodynamic setting of Northeast China and adjacent regions: closure of the Paleo-Asian Ocean and subduction of the Paleo-Pacific Plate. J. Asian Earth Sci. 26, 207–224. http://dx.doi.org/10.1016/j.jseaes.2005.09.001.

Li, Y., Wu, Q., Pan, J., Sun, L., 2012. S-wave velocity structure of northeastern China from joint inversion of Rayleigh wave phase and group velocities. Geophys. J. Int. 190, 105–115. http://dx.doi.org/10.1111/j.1365-246X.2012.05503.x.

Lin, F.-C., Ritzwoller, M.H., Yang, Y., Moschetti, M.P., Fouch, M.J., 2011. Complex and variable crustal and uppermost mantle seismic anisotropy in the western United States. Nat. Geosci. 4, 55–61. http://dx.doi.org/10.1038/ngeo1036.

Liu, Z., Huang, J., Peng, Z., Su, J., 2014. Seismic velocity changes in the epicentral region of the 2008 Wenchuan earthquake measured from three-component ambient noise correlation techniques. Geophys. Res. Lett. 41, 37–42. http://dx.doi.org/10.1002/2013GL058682.

Liu, Z., Niu, F., Chen, Y.J., Grand, S., Kawakatsu, H., Ning, J., Tanaka, S., Obayashi, M., Ni, J., 2015. Receiver function images of the mantle transition zone beneath NE China: new constraints on intraplate volcanism, deep subduction and their potential link. Earth Planet. Sci. Lett. 412, 101–111. http://dx.doi.org/10.1016/j.epsl.2014.12.019.

Long, M.D., Becker, T.W., 2010. Mantle dynamics and seismic anisotropy. Earth Planet. Sci. Lett. 297, 341–354. http://dx.doi.org/10.1016/j.epsl.2010.06.036.

Meng, Q.-R., 2003. What drove late Mesozoic extension of the northern China-Mongolia tract? Tectonophysics 369, 155–174. http://dx.doi.org/10.1016/S0040-1951(03)00195-1.

Montagner, J.-P., 1986. Regional three-dimensional structures using long-period surface waves. Ann. Geophys. 4 (B3), 283–294.

Montagner, J.-P., Tanimoto, T., 1991. Global upper mantle tomography of seismic velocities and anisotropies. J. Geophys. Res. 96, 20337. http://dx.doi.org/10.1029/91JB01890.

Oh, C.W., 2006. A new concept on tectonic correlation between Korea, China and Japan: histories from the late Proterozoic to Cretaceous. Gondwana Res. 9, 47–61. http://dx.doi.org/10.1016/j.gr.2005.06.001.

Priestley, K., Debayle, E., McKenzie, D., Pilidou, S., 2006. Upper mantle structure of eastern Asia from multimode surface waveform tomography. J. Geophys. Res. 111, B10304. http://dx.doi.org/10.1029/2005JB004082.

Ren, J., Tamaki, K., Li, S., Junxia, Z., 2002. Late Mesozoic and Cenozoic rifting and its dynamic setting in Eastern China and adjacent areas. Tectonophysics 344, 175–205. http://dx.doi.org/10.1016/S0040-1951(01)00271-2.

Sabra, K.G., Gerstoft, P., Roux, P., Kuperman, W.A., Fehler, M.C., 2005. Extracting time-domain Green's function estimates from ambient seismic noise. Geophys. Res. Lett. 32, L03310. http://dx.doi.org/10.1029/2004GL021862.

Savage, M.K., 1999. Seismic anisotropy and mantle deformation: what have we learned from shear wave splitting? Rev. Geophys. 37, 65–106. http://dx.doi.org/10.1029/98RG02075.

Seats, K.J., Lawrence, J.F., Prieto, G.A., 2012. Improved ambient noise correlation functions using Welch's method. Geophys. J. Int. 188, 513–523. http://dx.doi.org/10.1111/j.1365-246X.2011.05263.x.

Shapiro, N.M., Campillo, M., Stehly, L., Ritzwoller, M.H., 2005. High-resolution surface-wave tomography from ambient seismic noise. Science 307, 1615–1618. http://dx.doi.org/10.1126/science.1108339.

Smith, M.L., Dahlen, F.A., 1973. The azimuthal dependence of Love and Rayleigh wave propagation in a slightly anisotropic medium. J. Geophys. Res. 78, 3321–3333. http://dx.doi.org/10.1029/JB078i017p03321.

Tang, Y., Obayashi, M., Niu, F., Grand, S.P., Chen, Y.J., Kawakatsu, H., Tanaka, S., Ning, J., Ni, J.F., 2014. Changbaishan volcanism in northeast China linked to subduction-induced mantle upwelling. Nat. Geosci. 7, 470–475. http://dx.doi.org/10.1038/ngeo2166.

Tao, K., Niu, F., Ning, J., Chen, Y.J., Grand, S., Kawakatsu, H., Tanaka, S., Obayashi, M., Ni, J., 2014. Crustal structure beneath NE China imaged by NECESSArray receiver function data. Earth Planet. Sci. Lett. 398, 48–57. http://dx.doi.org/10.1016/j.epsl.2014.04.043.

Tarantola, A., Valette, B., 1982. Generalized nonlinear inverse problems solved using the least squares criterion. Rev. Geophys. 20, 219. http://dx.doi.org/10.1029/RG020i002p00219.

Wang, F., Zhou, X.-H., Zhang, L.-C., Ying, J.-F., Zhang, Y.-T., Wu, F.-Y., Zhu, R.-X., 2006. Late Mesozoic volcanism in the Great Xing'an Range (NE China): timing and implications for the dynamic setting of NE Asia. Earth Planet. Sci. Lett. 251, 179–198. http://dx.doi.org/10.1016/j.epsl.2006.09.007.

Wei, H., Liu, J.L., Meng, Q., 2010. Structural and sedimentary evolution of the southern Songliao Basin, northeast China, and implications for hydrocarbon prospectivity. Am. Assoc. Pet. Geol. Bull. 94, 533–566. http://dx.doi.org/10.1306/09080909060.

Wu, F.Y., Sun, D.Y., Ge, W.C., Zhang, Y..Bin., Grant, M.L., Wilde, S.A., Jahn, B.M., 2011. Geochronology of the Phanerozoic granitoids in northeastern China. J. Asian Earth Sci. 41, 1–30. http://dx.doi.org/10.1016/j.jseaes.2010.11.014.

Xu, W.-L., Pei, F.-P., Wang, F., Meng, E., Ji, W.-Q., Yang, D.-B., Wang, W., 2013. Spatial–temporal relationships of Mesozoic volcanic rocks in NE China: constraints on tectonic overprinting and transformations between multiple tectonic regimes. J. Asian Earth Sci. 74, 167–193. http://dx.doi.org/10.1016/j.jseaes.2013.04.003.

Xu, Y.-G., 2007. Diachronous lithospheric thinning of the North China Craton and formation of the Daxin'anling–Taihangshan gravity lineament. Lithos 96, 281–298. http://dx.doi.org/10.1016/j.lithos.2006.09.013.

Yang, Y., Ritzwoller, M.H., Levshin, A.L., Shapiro, N.M., 2007. Ambient noise Rayleigh wave tomography across Europe. Geophys. J. Int. 168, 259–274. http://dx.doi.org/10.1111/j.1365-246X.2006.03203.x.

Yao, H., Van Der Hilst, R.D., de Hoop, M.V., 2006. Surface-wave array tomography in SE Tibet from ambient seismic noise and two-station analysis-I. Phase velocity maps. Geophys. J. Int. 166, 732–744. http://dx.doi.org/10.1111/j.1365-246X.2006.03028.x.

Yao, H., Van der Hilst, R.D., 2009. Analysis of ambient noise energy distribution and phase velocity bias in ambient noise tomography, with application to SE Tibet. Geophys. J. Int. http://dx.doi.org/10.1111/j.1365-246X.2009.04329.x.

Yao, H., Van Der Hilst, R.D., Montagner, J.P., 2010. Heterogeneity and anisotropy of the lithosphere of SE Tibet from surface wave array tomography. J. Geophys. Res. Solid Earth 115, 1–24. http://dx.doi.org/10.1029/2009JB007142.

Zhang, F.Q., Chen, H.L., Yu, X., Dong, C.W., Yang, S.F., Pang, Y.M., Batt, G.E., 2011. Early Cretaceous volcanism in the northern Songliao Basin, NE China, and its geodynamic implication. Gondwana Res. 19, 163–176. http://dx.doi.org/10.1016/j.gr.2010.03.011.

Zhang, J.-H., Gao, S., Ge, W.-C., Wu, F.-Y., Yang, J.-H., Wilde, S.A., Li, M., 2010. Geochronology of the Mesozoic volcanic rocks in the Great Xing'an Range, northeastern China: implications for subduction-induced delamination. Chem. Geol. 276, 144–165. http://dx.doi.org/10.1016/j.chemgeo.2010.05.013.

Zhang, R., Wu, Q., Sun, L., He, J., Gao, Z., 2014. Crustal and lithospheric structure of Northeast China from S-wave receiver functions. Earth Planet. Sci. Lett. 401, 196–205. http://dx.doi.org/10.1016/j.epsl.2014.06.017.

Zheng, T., Chen, L., Zhao, L., Xu, W., Zhu, R., 2006. Crust-mantle structure difference across the gravity gradient zone in North China Craton: seismic image of the thinned continental crust. Phys. Earth Planet. Inter. 159, 43–58. http://dx.doi.org/10.1016/j.pepi.2006.05.004.

Zheng, X.-F., Yao, Z.-X., Liang, J.-H., Zheng, J., 2010. The role played and opportunities provided by IGP DMC of China National Seismic Network in Wenchuan Earthquake Disaster Relief and Researches. Bull. Seismol. Soc. Am. 100, 2866–2872. http://dx.doi.org/10.1785/0120090257.

Zheng, Y., Shen, W., Zhou, L., Yang, Y., Xie, Z., Ritzwoller, M.H., 2011. Crust and uppermost mantle beneath the North China Craton, northeastern China, and the Sea of Japan from ambient noise tomography. J. Geophys. Res. 116, 1–25. http://dx.doi.org/10.1029/2011JB008637.

Zhou, J.-B., Wilde, S.A., 2013. The crustal accretion history and tectonic evolution of the NE China segment of the Central Asian Orogenic Belt. Gondwana Res. 23, 1365–1377. http://dx.doi.org/10.1016/j.gr.2012.05.012.